Electron-enhanced atomic layer deposition of silicon thin films at room temperature

Jaclyn K. Sprenger, Huaxing Sun, and Andrew S. Cavanagh
Department of Chemistry and Biochemistry, University of Colorado, Boulder, Colorado 80309

Steven M. George[a)]
Department of Chemistry and Biochemistry, University of Colorado, Boulder, Colorado 80309 and Department of Mechanical Engineering, University of Colorado, Boulder, Colorado 80309

(Received 27 September 2017; accepted 30 November 2017; published 27 December 2017)

Silicon thin films were deposited at room temperature with electron-enhanced atomic layer deposition (EE-ALD) using sequential exposures of disilane (Si_2H_6) and electrons. EE-ALD promotes silicon film growth through hydrogen electron stimulated desorption (ESD) that creates reactive dangling bonds and facilitates Si_2H_6 adsorption at low temperatures. Without hydrogen ESD, silicon growth relies on thermal pathways for H_2 desorption and dangling bond formation at much higher temperatures. An electron flood gun was utilized to deposit Si films over areas of $\sim$1 cm^2 on oxide-capped Si(111) substrates. The silicon film thickness was monitored *in situ* with a multiwavelength ellipsometer. A threshold electron energy of $\sim$25 eV was observed for the Si film growth. A maximum growth rate of $\sim$0.3 Å/cycle was measured at electron energies of 100–150 eV. This growth rate is close to the anticipated growth rate assuming dissociative Si_2H_6 adsorption on dangling bonds on representative single-crystal silicon surfaces. The Si growth rate also displayed self-limiting behavior as expected for an ALD process. The silicon growth rate was self-limiting at larger Si_2H_6 pressures for a fixed exposure time and at longer electron exposure times. The silicon growth rate versus electron exposure time yielded a hydrogen ESD cross section of $\sigma = 5.8 \times 10^{-17}$ cm^2. *Ex situ* spectroscopic ellipsometry showed good conformality in thickness across the $\sim$1 cm^2 area of the Si film. Si EE-ALD should be useful for a variety of applications. *Published by the AVS*. https://doi.org/10.1116/1.5006696

I. INTRODUCTION

Silicon is one of the most important semiconductor materials and is foundational for microelectronic devices. Silicon is usually deposited by chemical vapor deposition (CVD) at high temperatures ranging from 600 to 1100 °C with various silane and chlorosilane precursors.[1–5] At the low end of this temperature range, the silicon growth rate is dominated by surface kinetic processes.[1,2] At the high end of this temperature range, the silicon growth rate is determined by reactant mass transport.[1,2]

The surface kinetic processes that limit silicon growth at low temperatures are either H_2 desorption using silane precursors or HCl desorption using chlorosilane precursors.[1–3] The strong Si–H bond energy of $\sim$90 kcal/mol and the recombinatory H_2 kinetics lead to high desorption temperatures.[6–8] The desorption temperatures are $\sim$370–600 °C for H_2 desorption from dihydride and monohydride species.[6,7,9–11] The minimum Si growth temperatures using silanes are correlated with the H_2 desorption required to create dangling bonds that can adsorb additional silane precursors resulting in silicon growth.[3]

Silicon growth could occur at much lower temperatures if hydrogen could be desorbed by nonthermal means. One possible nonthermal hydrogen desorption mechanism is electron stimulated desorption (ESD).[12–14] ESD can occur through a number of processes such as the Menzel–Gomer–Redhead and Knotek–Feibelman mechanisms.[15–18] ESD has been previously used for surface analysis to image chemical bond directionality and thermal disorder in adsorbed species using electron stimulated desorption ion angular distribution (ESDIAD techniques).[19–25] ESD is also a component of electron beam induced deposition which uses high energy electrons for the direct writing of nanostructures.[26] However, ESD has not been used for macroscopic thin film growth.

Hydrogen removal by ESD from silicon surfaces has also been achieved using scanning tunneling microscopy (STM) techniques.[27–29] STM-ESD desorbs hydrogen with a different mechanism and leaves behind dangling bonds on the silicon surface.[27–32] These dangling bonds are very reactive and readily adsorb other precursors. The remaining hydrogen acts as a mask to prevent adsorption and provides a pathway for hydrogen desorption nanolithography.[32] The dangling bonds can be reacted with precursors to form nanoscale features such as oxide,[27,33] Fe,[28] and TiO_2 (Ref. 34) nanoscale lines on Si(100) surfaces. Multiple Si monolayers over nanoscale areas of 100×100 nm^2 have also been fabricated on Si(100) using sequential hydrogen ESD and disilane exposures.[35,36]

GaN electron-enhanced growth was recently performed to demonstrate the feasibility of electron-enhanced macroscopic thin film growth.[37] GaN CVD usually requires temperatures of 800–1100 °C using precursors such as $Ga(CH_3)_3$ and NH_3.[38–40] For GaN electron-enhanced growth, film growth was performed at much lower temperatures of room temperature and 100 °C using sequential reaction cycles with

a)Electronic mail: Steven.George@Colorado.edu

$Ga(CH_3)_3$, H radical, NH_3, and electron exposures.[37] GaN growth rates up to 1.3 Å/cycle were observed for electron energies of 50 eV. In addition, x-ray diffraction and transmission electron microscopy measurements revealed that the GaN films were polycrystalline.[37]

In this paper, sequential exposures of Si_2H_6 and low energy electrons are used to grow silicon films over areas of ~1 cm^2 by electron-enhanced atomic layer deposition (EE-ALD) at room temperature. The Si EE-ALD films were grown in a stepwise sequence as illustrated in Fig. 1. The silicon growth rate was measured using *in situ* ellipsometry as a function of electron energy up to 200 eV. Silicon growth was also studied versus Si_2H_6 and electron exposures to determine if the sequential reactions are both self-limiting. In addition, the film composition was evaluated using *in situ* Auger electron spectroscopy (AES) and *ex situ* x-ray photoelectron spectroscopy (XPS). These studies demonstrate that nonthermal desorption of hydrogen using ESD can be used to deposit silicon films at room temperature.

II. EXPERIMENT

A. Vacuum chamber

The silicon films were grown in a vacuum chamber that is similar to the vacuum chamber that has been described previously.[37] This experimental apparatus contains a sample load lock, a main vacuum chamber pumped with an ion pump and a turbomolecular pump, and a sample analysis chamber containing an AES spectrometer that is pumped with an ion pump. A schematic of this experimental apparatus is shown in Fig. 2. The main chamber also contains an electron gun (Model FRA-2x1-2, Kimball Physics, Inc.), a mass spectrometer (PrismaPlus QMG 220, Pfeiffer Vacuum) and hot cathode and cold cathode pressure gauges. The sample analysis chamber also includes a hot cathode pressure gauge.

Compared with the previous study of electron-enhanced GaN thin film growth,[37] the electron flood gun in this investigation was oriented normal to the substrate surface. In addition, a different cathode material was used in the electron gun. The cathode filament assembly was comprised of a tantalum disk secured to a tungsten-rhenium (95%–5%) support. The filament assembly used for the earlier demonstration of

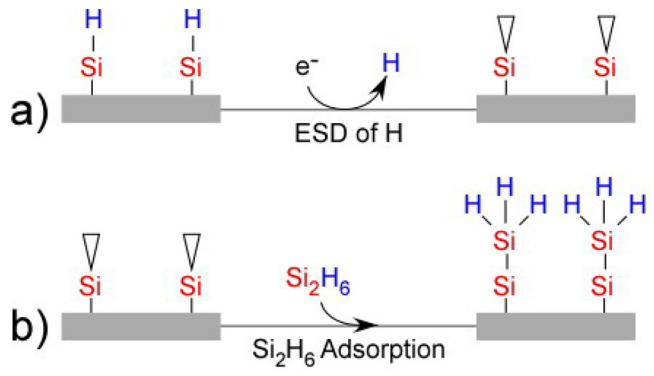

FIG. 1. (Color online) Proposed growth mechanism for Si EE-ALD using disilane as the reactant.

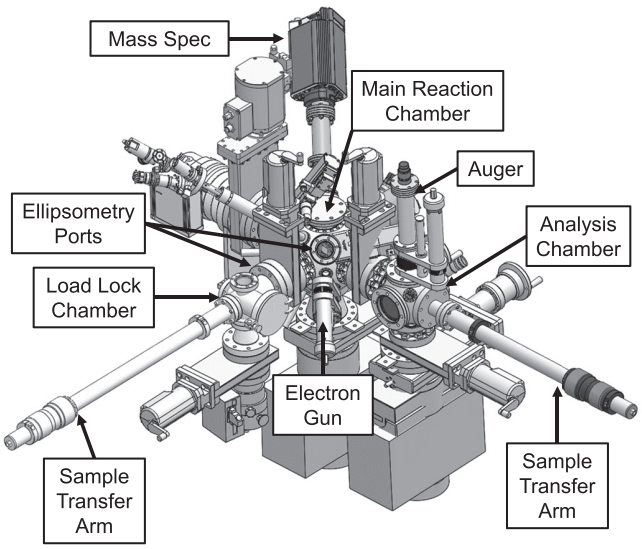

FIG. 2. Schematic of experimental apparatus showing sample load lock, main chamber and sample analysis chamber.

electron-enhanced GaN film growth was composed of an yttria-coated iridium disk on an iridium support.[37] The electron flood gun produced electron energies from 5 to 1000 eV at electron currents of 1 nA to 400 μA.

Some additional experimental changes were also made compared with the earlier study of electron-enhanced GaN growth.[37] The hydrogen atom beam source (HABS) (MBE-Komponenten GmbH) was moved to the surface analysis chamber for initial substrate surface cleaning. The new location for the HABS placed the hydrogen radical outlet within 1 cm of the substrate and normal to the surface. This location greatly increased the flux of hydrogen radicals to the surface and produced more efficient surface cleaning.

B. Growth procedure

Si films were grown using disilane (Si_2H_6; 99.998%, Voltaix). Films were deposited on boron-doped Si (111) substrates (Silicon Valley Microelectronics, Inc.) that had been capped with either an Al_2O_3 ALD thin film or a $Zn_{0.55}Mg_{0.45}O$ ALD thin film grown in a different reactor. These buffer films were employed to facilitate analysis of the Si films using the compositional analysis techniques. Prior to loading in the reaction chamber, the substrates were rinsed with acetone and methanol, and then dried with N_2.

Substrates were loaded into the load lock chamber and the background pressure was reduced to 1×10^{-6} Torr. The chamber and substrate were irradiated with a UV lamp for 30 min (mini-Z, RBD Instruments) to desorb water from the substrate surface and chamber walls. After the pressure in the load lock chamber was reduced to approximately 1×10^{-8} Torr, the substrate and sample stage were transferred into the main chamber. The main chamber and substrate were irradiated with UV light for 30 min. After irradiation, the substrate was transferred to the analysis chamber and exposed to hydrogen radicals created by the HABS using hydrogen gas (H_2; research grade, Airgas) at 1×10^{-5} Torr for 30 min. The hydrogen radical flux

at the surface was estimated to be 5×10^{15} atoms $cm^{-2} s^{-1}$. The substrate was then returned to the main chamber for the growth experiments. The EE-ALD was performed after the main chamber reached a base pressure of 5×10^{-10} Torr.

The Si substrate was exposed to electrons with an energy of 0–200 eV for 0–480 s. The electron current emitted from the electron gun during electron exposures was 100 μA for the growth experiments. All reactions were performed at room temperature (27 °C). The Si_2H_6 exposures were defined by pressure transients of 0–0.4 mTorr for <300 ms. These Si_2H_6 exposures were created using Si_2H_6 pressures of 0–10 Torr behind a pulsed valve (Parker Hannifin Corp.). The pulsed valve was open for 100 ms. Chamber pressures >0.4 mTorr caused the *in situ* cold cathode gauge to shut off and were not quantifiable.

Silicon CVD from Si_2H_6 on the electron gun filament assembly composed of a yttria-coated iridium disk on an iridium support progressively led to the formation of silicides. Eventually, the filament assembly failed and required replacement. The filament assembly was changed to a tanatlum disk on a tungsten-rhenium support to mitigate this problem. In addition, as a precaution to prolong the life of the filament assembly, sufficient time was given to allow the filament to cool to prevent Si CVD. The minimum Si CVD temperature is ~400 °C.[41] Achieving filament temperatures of <400 °C was the goal of these wait times.

A typical EE-ALD reaction sequence consisted of an electron gun exposure at 100 eV for 60 s with an electron emission current of 100 μA. A 300 s wait time was conducted to allow the electron gun filament to cool sufficiently. The surface was then exposed to a disilane dose of approximately 0.15 mTorr for <300 ms. A 30 s purge was performed to clear the chamber of disilane precursor. Three *in situ* ellipsometry scans of 1 s each were then recorded to determine the silicon film thickness. Another 120 s was utilized to allow the electron gun filament to warm up to temperature. This sequence was then repeated to reach the desired film thickness. These repeating sequences were automated using LABVIEW. Approximately 8.5 min were required to complete one full cycle of Si EE-ALD.

The time for one full cycle of Si EE-ALD could be shortened by utilizing high current plasma electron sources.[42] These plasma electron sources would eliminate the wait times for the electron gun filament to cool and to warm up. In addition, the speed for one Si EE-ALD cycle could be faster using spatial ALD techniques.[43] Sample translation during spatial ALD leads to shorter times between the sequential surface reactions. A spatial EE-ALD reactor has been constructed using a DC glow discharge plasma electron source. The results of this spatial EE-ALD reactor for Si EE-ALD will be discussed in a future publication.

C. *In situ* film analysis

The reaction chamber was equipped with an *in situ* four-wavelength ellipsometer (FS-1, Film Sense) to measure the film thickness and film growth rate. Measurements were performed at an incidence angle of 55°. Prior to the EE-ALD, a scan of the substrate was recorded to establish the baseline. The film growth was determined using a Cauchy model. During growth, three consecutive 1 s scans were collected after each Si_2H_6 exposure. Film thicknesses obtained from these three scans were averaged together to determine the film thickness after each Si_2H_6 exposure. Growth rates were determined from film thicknesses over five reaction cycles for each set of reaction parameters. The plots of thickness versus number of EE-ALD cycles were linear.

Film composition was determined with *in situ* AES (microCMA, RBD Instruments). The AES spectrometer scanned a kinetic energy range of 30–730 eV with a step size of 1 eV. The electron beam potential was 2.5 kV with a filament current of 2.6 A. The AES data was collected and processed using CMapp (RBD Instruments) software.

D. *Ex situ* film analysis

The Si films were analyzed using a variety of *ex situ* techniques. Additional film thickness measurements were performed using spectroscopic ellipsometry (SE) with a spectroscopic ellipsometer (Model M-2000, J.A. Woollam Co., Inc.). This ellipsometer was equipped with focusing probes that reduced the beam size to ~300–400 μm and allowed for spatial mapping of the ~1 cm^2 growth area. Data were collected at 65° and 70° incidence angles. The SE data was fitted with a Cody–Lorentz model using CompleteEase (J.A. Woollam Co., Inc.) software. The large number of wavelengths from the *ex situ* SE data allowed the use of the more detailed Cody–Lorentz model.

The film composition was determined by XPS analysis using an x-ray photoelectron spectrometer (PHI 5600). The spectrometer used a monochromatic Al-Kα source at 1486.6 eV. The pass energy was 29.35 eV and the step size was 0.25 eV. An electron beam neutralizer was used during the XPS measurements. XPS depth-profiling and surface carbon removal was conducted using argon ion sputtering. The XPS data was collected using AUGER SCAN (RBD Instruments) software. The XPS data was analyzed in CASA XPS (Casa Software, Ltd.) software.

The Si films were studied using grazing incidence x-ray diffraction (GIXRD) to determine if the films were crystalline. These GIXRD studies were performed with an x-ray diffractometer (D1 System, Bede Scientific, Inc.). The GIXRD utilized Cu-Kα irradiation at an incidence angle of 0.3°.

III. RESULTS AND DISCUSSION

A. Film growth and characterization using *in situ* four-wavelength ellipsometry

The film thicknesses versus number of EE-ALD cycles are shown in Fig. 3. These *in situ* measurements were performed after each Si_2H_6 exposure. The reaction conditions consisted of an electron energy of 50 eV, electron exposure times of 60 s, and Si_2H_6 doses of 0.15 mTorr for <300 ms. After a nucleation delay, the film thickness versus number of EE-ALD cycles was linear. The growth rate of 0.15 Å/cycle

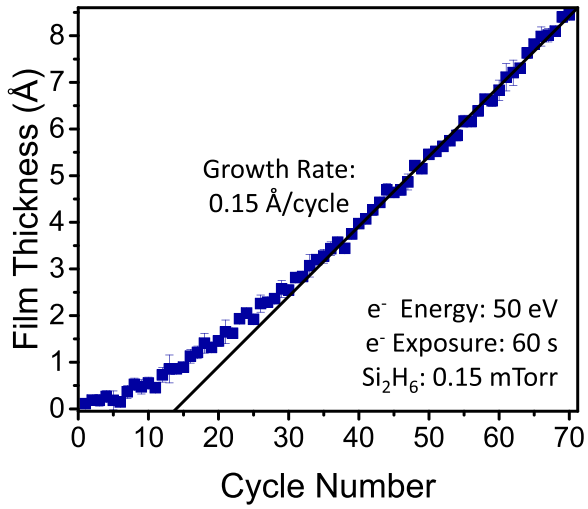

FIG. 3. (Color online) Si EE-ALD on an Al_2O_3/Si(111) substrate at 27 °C displaying a growth rate of 0.15 Å/cycle after an initial nucleation period of ~35 cycles. Electron energy was 50 eV, electron exposure time was 60 s, and Si_2H_6 dose pressure was 0.15 mTorr for <300 ms.

was determined by fitting the linear portion of the data in Fig. 3. This growth rate is consistent with submonolayer silicon growth.

Figure 3 shows that there is a slight nucleation delay of ~35 cycles when the silicon films are grown on a Si(111) substrate that had been capped with an Al_2O_3 ALD film with a thickness of ~200 Å. The Si EE-ALD may nucleate by the adsorption of Si_2H_6 on Al-OH species on the Al_2O_3 ALD surface.[44] The electron exposures may also remove hydrogen or other surface species from the Al_2O_3 ALD surface and form reactive sites. These reactive sites may then allow Si_2H_6 adsorption.

The growth rate of the Si films was dependent on the electron energy used for hydrogen ESD. Figure 4 shows the film thickness versus cycle number for electron energies of 30, 88, and 150 eV. The experiments were performed with electron exposure times of 60 s and Si_2H_6 dose pressures of 0.15 mTorr for <300 ms. The film thickness versus cycle number is linear. The silicon growth rate is larger at the higher electron energies. Silicon growth rates of approximately 0.1, 0.2, and 0.3 Å/cycle were obtained at 30, 88, and 150 eV, respectively.

Figure 5 summarizes the silicon growth rate dependence on electron energy from 0 to 200 eV. Measurements are displayed for two separate sample sets and illustrate the reproducibility of the results. The silicon growth was linear at all of the electron energies. All experiments were performed with electron exposure times of 60 s and Si_2H_6 dose pressures of 0.15 mTorr for <300 ms.

Little to no Si film growth is observed until reaching the threshold for silicon growth at an electron energy of ~25 eV. The threshold for silicon growth at ~25 eV is close to the measured threshold for hydrogen ESD from silicon at ~23 eV.[13,45–47] This threshold is believed to represent the energy required to excite two holes into Si–H valance bonds. This excitation yields hydrogen desorption and leaves behind a dangling bond.[13,45,46]

Figure 5 reveals that the silicon growth rate is ~0.15 Å/cycle between 50 and 80 eV before increasing rapidly around 85–90 eV. An increase in hydrogen ESD from silicon was also measured earlier at ~100 eV.[13] This increase is likely correlated with the Si 2p core-level binding energy at 99 eV. Desorption of hydrogen at this energy is attributed to electron removal from the Si 2p core level and an Auger decay to the Si 2p core level leaving a hole in the Si–H bond.[13]

A fairly constant silicon growth rate of ~0.27 Å/cycle is measured between 100 and 150 eV. Subsequently, Fig. 5 shows that there is a decrease in the silicon growth rate at ~155 eV. In contrast, there is a corresponding increase in the hydrogen ESD from silicon.[13] This increase was attributed to electron removal from the Si 2s core level and an Auger decay to the Si 2s core level at 150 eV that desorbs hydrogen. For the silicon growth rates shown in Fig. 5, the Auger

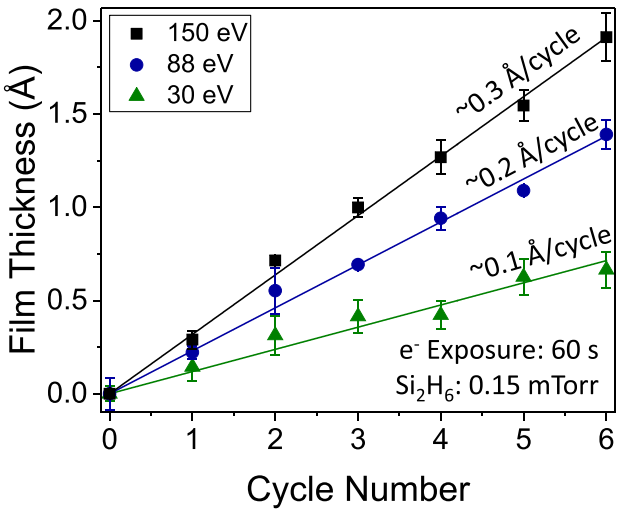

FIG. 4. (Color online) Film thickness vs number of reaction cycles for electron energies of 30, 88 and 150 eV at 27 °C. Electron exposure time was 60 s and Si_2H_6 dose pressure was 0.15 mTorr for <300 ms.

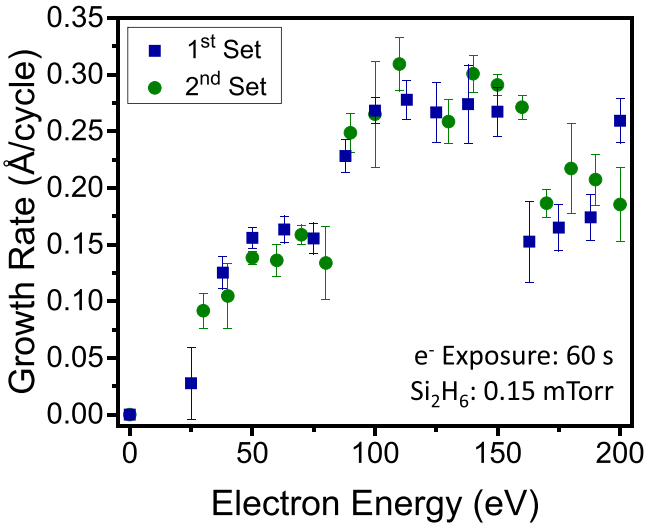

FIG. 5. (Color online) Growth rate for Si EE-ALD films at 27 °C vs electron energy. Electron exposure time was 60 s and Si_2H_6 dose pressure was 0.15 mTorr for <300 ms.

decay to the Si 2s core level is believed to desorb Si species in addition to hydrogen. This competing Si etch process is observed as a decrease in the silicon growth rate.

B. Self-limiting growth characterization

Experiments were performed to determine if the silicon growth rate was self-limiting at larger Si_2H_6 exposures. These investigations were conducted by varying the Si_2H_6 pressure behind the pulsed valve from 1 to 10 Torr for a valve open time of 100 ms. These Si_2H_6 doses resulted in chamber pressure excursions of 0–0.4 Torr for <300 ms. Experiments were also performed to determine if the silicon growth was self-limiting at longer electron exposure times. These investigations varied the electron exposure time at a constant electron current with an electron energy of 100 eV.

Figure 6 shows the dependence of the silicon growth rate on the Si_2H_6 dose pressure for a Si_2H_6 pressure transient of <300 ms. As the Si_2H_6 dose pressure increases, there is a corresponding increase in silicon growth rate until self-limiting behavior is observed for Si_2H_6 dose pressures greater than 0.15 mTorr. The limiting factor is believed to be the consumption of available dangling bonds. After Si_2H_6 exposures sufficient to react with all of the available dangling bonds, there is no additional increase in the silicon growth rate at higher Si_2H_6 dose pressures.

Figure 7 displays the silicon growth rate versus the electron exposure time. These measurements were again performed with an electron energy of 100 eV and electron exposure times of 60 s. The Si_2H_6 dose pressure was 0.15 mTorr for <300 ms. The silicon growth rate increases rapidly with electron exposure time and levels off at ~0.32 Å/cycle for electron exposure times longer than 120 s. This self-limiting behavior is believed to result from the production of a limiting number of dangling bonds that can adsorb Si_2H_6 during the subsequent Si_2H_6 exposure.

The silicon growth rate of ~0.32 Å/cycle obtained from the results in Fig. 7 is the maximum silicon growth rate

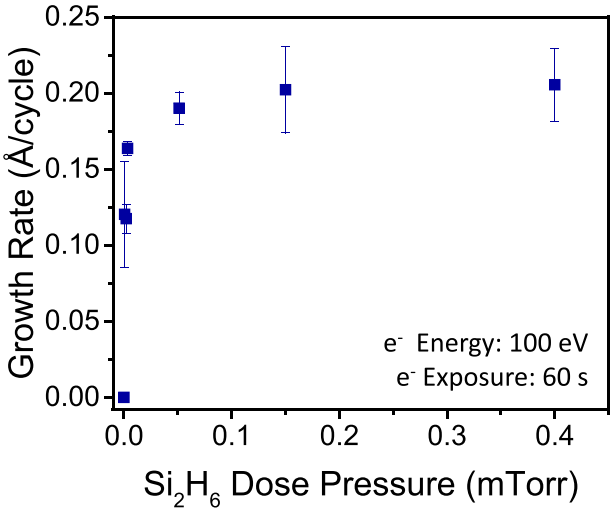

FIG. 6. (Color online) Growth rate of Si EE-ALD films at 27 °C vs Si_2H_6 dose pressures for exposure times of <300 ms. Electron energy was 100 eV and electron exposure time was 60 s.

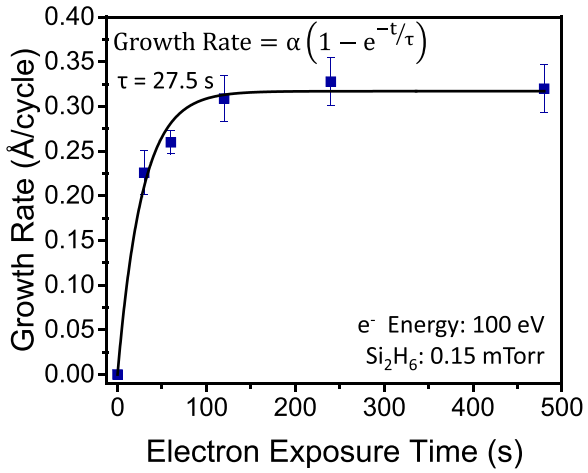

FIG. 7. (Color online) Growth rate of Si EE-ALD films at 27 °C vs electron exposure times. Electron energy was 100 eV and Si_2H_6 dose pressure was 0.15 mTorr for <300 ms. Silicon growth rate was proportional to $(1 - e^{-t/\tau})$. Hydrogen ESD cross section determined from τ was $\sigma = 5.8 \times 10^{-17}$ cm^2.

given the available reaction parameters. This silicon growth rate can be compared with the silicon growth rate measured earlier using STM-ESD to desorb hydrogen followed by disilane adsorption on the dangling bonds. Sequential cycles of hydrogen desorption from Si(100) by STM-ESD and disilane adsorption produced silicon growth rates of ~0.43 Å/cycle.[35] This silicon growth rate is close to the silicon growth rate of ~0.32 Å/cycle obtained from Fig. 7.

The slightly smaller growth rate for EE-ALD may reflect the differences between the Si(100) surface used in the STM-ESD work and the silicon surfaces in this work. In addition, the hydrogen ESD was conducted at 7 eV in the STM-ESD experiments compared with the electron energies of 100 eV for the results in Fig. 7. The mechanism for STM-ESD at these lower electron energies is believed to involve multiple vibrational excitation of the Si–H bond.[31] The different electron energies and ESD desorption cross sections may affect the amount of hydrogen that can be desorbed from the silicon surfaces. Fewer dangling bonds on the silicon surface would lead to less Si_2H_6 adsorption and lower silicon growth rates.

Disilane (Si_2H_6) will dissociatively adsorb on dangling bonds on silicon surfaces. At room temperature and lower temperatures, Si_2H_6 will adsorb and produce SiH_3 and SiH_2 features in the infrared absorption vibrational spectrum.[48,49] Based on the vibrational spectra and identical measured sticking coefficients for Si_2H_6 and Si_2D_6 on Si(100) and Si(111) 7×7 surfaces, disilane is believed to dissociatively adsorb by breaking the Si-Si bond to produce $–SiH_3$ surface surfaces.[50,51] However, some infrared absorption studies and theoretical analysis also suggests that Si_2H_6 can adsorb by breaking a Si–H bond to produce Si–H and Si–Si_2H_5 surface species.[52,53]

Both Si–Si and Si–H bond-breaking adsorption pathways for Si_2H_6 would require at least two nearby dangling bonds on the silicon surface. The silicon growth rate of ~0.32 Å/cycle can be used to estimate the number of dangling bonds on the silicon surface that react with Si_2H_6 assuming that

each Si_2H_6 molecule that adsorbs requires two dangling bonds. The silicon growth of ~0.32 Å/cycle is consistent with the deposition of 1.6×10^{14} Si/cm^2 per cycle assuming a silicon number density of 5.0×10^{22} Si/cm^3. A deposited silicon coverage of 1.6×10^{14} Si/cm^2 per cycle would require at least 1.6×10^{14} dangling bonds/cm^2 per cycle.

This required dangling bond coverage of 1.6×10^{14} dangling bonds/cm^2 per cycle is less than the dangling bond coverage of 3.4×10^{14} dangling bonds/cm^2 on the reconstructed Si(100) 2×1 surface and 3.1×10^{14} dangling bonds/cm^2 on the reconstructed Si(111) 7×7 surface. However, the $-SiH_3$ species may decompose further upon adsorption to produce additional hydrogen by $SiH_3 \rightarrow SiH_2 + H$.[2,3,48] This decomposition would require additional dangling bonds and a total dangling bond coverage of at least 3.2×10^{14} dangling bonds/cm^2. For comparison, this estimated required dangling bond coverage is close to the dangling bond coverage on the reconstructed Si(100) 2×1 and Si(111) 7×7 surfaces.

C. Hydrogen ESD cross section

The hydrogen ESD cross section at 100 eV can be determined from the silicon growth rate versus electron exposure time at 100 eV presented in Fig. 7. This determination assumes that the silicon growth is occurring as the result of hydrogen ESD producing dangling bonds. These dangling bonds then react with Si_2H_6 molecules to produce silicon growth. If there are no dangling bonds produced by hydrogen ESD, then no silicon growth should occur. This behavior was confirmed by control experiments where the electron exposures were replaced with a wait time and every other reaction step remained the same. These control experiments revealed that the electrons were essential for silicon growth.

Assuming that the silicon surface is hydrogen terminated, hydrogen ESD produces a coverage of dangling bonds that is inversely proportional to the hydrogen surface coverage, Θ_H. The rate of change in the hydrogen surface coverage during hydrogen ESD can be described by[54,55]

$$d\Theta_H/dt = -\Phi\sigma\Theta_H. \quad (1)$$

In Eq. (1), Φ is the electron flux across the surface (e^-/cm^2 s), σ is the total hydrogen desorption cross section (cm^2), and $\Theta_H(t)$ represents the hydrogen surface coverage as a function of time. Solving the above differential equation results in

$$\Theta_H/\Theta_{H0} = \exp(-\Phi\sigma t), \quad (2)$$

where Θ_{HO} is the initial hydrogen coverage. Equation (2) can be rewritten in terms of the time constant, τ, in (s), where $\tau = (1/\Phi\sigma)$. This definition of τ yields

$$\Theta_H/\Theta_{H0} = \exp(-t/\tau). \quad (3)$$

Equation (3) describes the hydrogen coverage on the surface. The remaining coverage should be comprised of dangling bond sites. Therefore, the dangling bond coverage Θ_{DB} can be expressed as

$$\Theta_{DB}/\Theta_{DB0} = 1 - \exp(-t/\tau), \quad (4)$$

where Θ_{DBO} is the maximum dangling bond coverage which is equivalent to Θ_{HO}. This treatment assumes that the dangling bond sites produced by hydrogen ESD do not undergo reconstruction.

Based on the initial assumption that the silicon growth rate is proportional to the dangling bond coverage given by Eq. (4), the silicon growth rate, R_{Si}, is

$$R_{Si} = \alpha[1 - \exp(-t/\tau)]. \quad (5)$$

In Eq. (5), α represents the maximum silicon growth rate assuming ideal conditions with no reactants besides Si_2H_6 competing for the dangling bonds. The experimental results in Fig. 7 at 100 eV can be fit by Eq. (5). The line in Fig. 7 shows the fit with $\alpha = 0.32$ Å/cycle and $\tau = 27.5$ s.

The electron stimulated hydrogen desorption cross section can then be obtained from these fitting parameters. The earlier definition of $\tau = (1/\Phi\sigma)$ can be rearranged to yield an equation for the cross section

$$\sigma = 1/\Phi\tau. \quad (6)$$

In Eq. (6), the electron flux is defined as $\Phi = I/Ae$, where I is the electron current, A is the electron beam area, and e is the charge of an electron. In these experiments, $I = 100$ μA and $A = 1$ cm^2. Using these experimental parameters together with τ from the fit to Fig. 7, the hydrogen ESD cross section at 100 eV is $\sigma = 5.8 \times 10^{-17}$ cm^2.

As a comparison, the hydrogen ESD cross section measured on Si(100) at 100 eV is $\sigma = 7 \times 10^{-19}$ cm^2.[13] The hydrogen ESD cross section measured on Si(111) at 100 eV is $\sigma = 9 \times 10^{-20}$ cm^2.[12] The deuterium ESD cross section is lower than the hydrogen ESD cross section. The deuterium ESD cross section measured on Si(111) at 100 eV is $\sigma = 2 \times 10^{-21}$ cm^2.[14] Additional STM measurements of the ESD cross section at lower electron energies of 7–30 eV on Si(100) are $\sigma = 3 \times 10^{-20}$–$4 \times 10^{-21}$ for hydrogen and $\sigma = 7 \times 10^{-23}$ for deuterium.[28,29,31]

The hydrogen ESD cross section of $\sigma = 5.8 \times 10^{-17}$ cm^2 measured in this study is over 80 times larger than the hydrogen ESD cross section of $\sigma = 7 \times 10^{-19}$ cm^2 measured on Si(100). The reason for this difference is not known at this time. One possibility is that the hydrogen ESD cross section is sensitive to the underlying structure of the silicon surface. Single-crystal silicon surfaces were employed in the previous investigations. The degree of crystallinity of the Si EE-ALD films is not known and the silicon films may have been amorphous. In addition, the silicon surfaces in this EE-ALD study contained carbon impurities at a concentration of ~10 at. % as discussed in Sec. III D. Surface impurities may influence the hydrogen ESD cross section.

D. Composition from *in situ* AES and *ex situ* XPS depth-profiling measurements

The surface composition of the Si film was established by *in situ* AES measurements. Prior to Si EE-ALD deposition, the AES scans of the surface showed only Al and O AES signals from the Al_2O_3 ALD buffer film with some carbon

impurities. The Si AES signal from the underlying Si(111) wafer was below the AES detection limit. After 1300 cycles of Si EE-ALD film growth at room temperature, a strong Si AES peak was observed at 93 eV as shown in Fig. 8. The Al AES signal was below the detection limit. The loss of the Al AES signal is expected because the Si EE-ALD film has a thickness of 185 Å as determined from *in situ* ellipsometry.

In addition to the strong Si AES peak, Fig. 8 also observes O and C impurities at 6 and 21 at. %, respectively. The C impurities may result from hydrocarbon adsorption on the dangling bonds formed by hydrogen ESD. However, the level of C impurities increased with each successive AES scan. Little increase in the C impurities was observed when the sample resided in the chamber for 24 h. This behavior led to the conclusion that the electron filament within the AES spectrometer was at least partly responsible for producing carbon species that adsorbed onto the surface.

Figure 9 shows the *ex situ* XPS depth profile for a Si EE-ALD film grown at room temperature using 1000 Si EE-ALD reaction cycles on a $Zn_{0.55}Mg_{0.45}O$ ALD thin film on the Si(111) wafer. This Si film had an initial thickness of ~250 Å. The *ex situ* XPS scans reveal an oxidized silicon film resulting from atmospheric exposure. The XPS measurement of ~25 at. % for the oxygen concentration in the bulk of the Si EE-ALD film is higher than the AES measurement of ~6 at. % for the oxygen concentration on the surface of the Si EE-ALD film. This higher concentration of oxygen may indicate that the Si EE-ALD film has a lower density than crystalline silicon. The refractive index is dependent on density according to the Lorentz–Lorenz formula. The refractive index of the Si EE-ALD film determined by the *in situ* four-wavelength ellipsometer was n ~ 3.009 at 633 nm (1.96 eV). In comparison, crystalline Si has a refractive index of n = 3.847 at 653 nm (1.9 eV) and n = 3.906 at 620 nm (2.0 eV).[56]

Figure 9 also reveals that carbon is observed at ~10 at. % throughout the Si film. This result confirms that the *in situ* AES measurements were influenced by carbon produced by the AES measurements. The XPS measurements of ~10 at. % for the carbon concentrations are more representative of the Si EE-ALD growth. Carbon could originate from residual hydrocarbons in the vacuum chamber that compete with disilane for the dangling bonds after hydrogen ESD. Mass spectrometry measurements observed low levels of methyl and other carbon species in the vacuum chamber. These species also increased in pressure during the electron exposures with the hot electron gun filament.

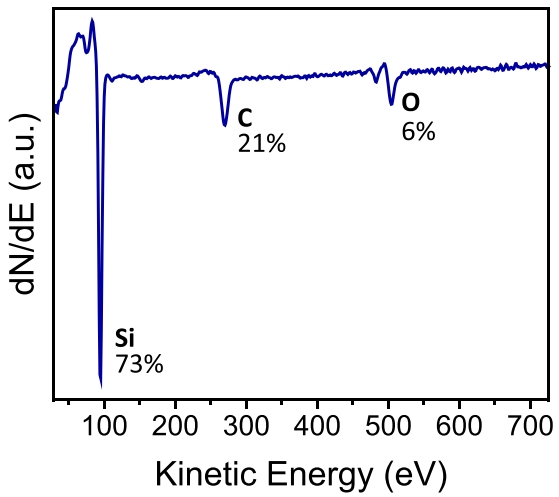

FIG. 8. (Color online) AES analysis of film grown using 1300 Si EE-ALD reaction cycles at 27 °C. Electron energy was 100 eV, electron exposure time was 60 s, and Si_2H_6 dose pressure was 0.15 mTorr for <300 ms.

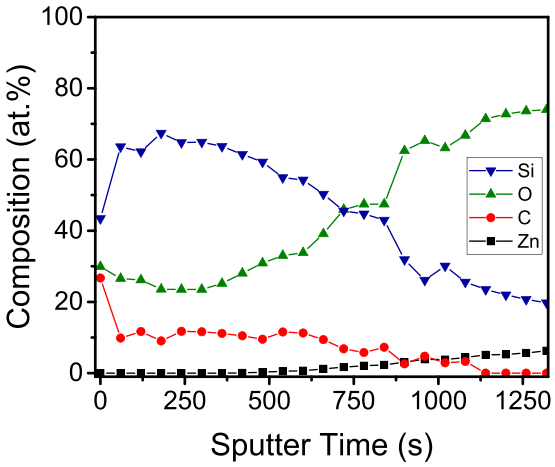

FIG. 9. (Color online) XPS depth-profile of film grown on Si(111) wafer at 27 °C with a $Zn_{0.55}Mg_{0.45}O$ ALD buffer layer using 1000 Si EE-ALD reaction cycles. Electron energy was 100 eV, electron exposure time was 60 s, and Si_2H_6 dose pressure was 0.15 mTorr for <300 ms.

E. Spatial profile of deposition area and XRD measurements

The Si EE-ALD films are dependent on the electron flux to the surface as demonstrated in Fig. 7. The Si film grew only where the electron flux was present. Figure 10 shows a

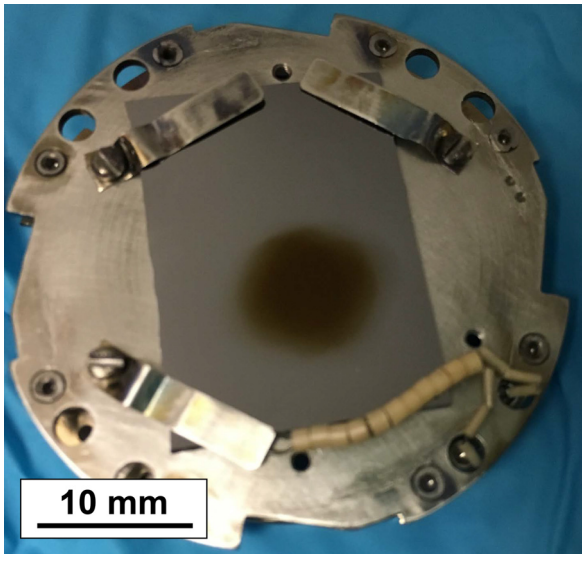

FIG. 10. (Color online) Photo of growth area on Si(111) wafer with a ~200 Å Al_2O_3 ALD buffer layer. Film was grown using 1350 Si EE-ALD reaction cycles at 27 °C. Electron energy was 50 eV, electron exposure time was 60 s, and Si_2H_6 dose pressure was 0.15 mTorr for <300 ms.

picture of the Si film on the Si(111) wafer attached to the sample stage. This Si film was grown using 1350 cycles of Si EE-ALD with an electron energy of 50 eV, electron exposure time of 60 s and Si_2H_6 dose pressure of 0.15 mTorr for <300 ms. The deposited silicon film is visible as a circular ~1 cm^2 area on the Al_2O_3 ALD film on the Si(111) surface. The Si film is dark brown in color. The silicon growth area is symmetric resulting from the incident electron flux at the surface normal and the Gaussian spatial distribution of the electron beam. Previous studies of GaN electron-enhanced growth observed growth areas that were not symmetric because the electron beam was incident on the substrate at 55° from the surface normal.[37]

Ex situ spectroscopic ellipsometry was also used to measure the film thickness and spatial profile across the Si(111) wafer. Figure 11 shows the thickness profile for the growth area observed in Fig. 10. The Si film has a thickness of ~140 Å. The Si EE-ALD growth rate determined from this thickness was 0.14 Å/cycle. This Si EE-ALD growth rate is consistent with the Si EE-ALD growth rate observed at 50 eV in Fig. 5.

Figure 11 reveals that the Si film shows a thickness variation of <10 Å across the ~1 cm^2 growth area. In addition, there is a sharp decrease in Si film thickness near the edge of the growth area. This fairly "flat top" with steep edges suggests that the hydrogen ESD has produced a self-limiting dangling bond coverage over much of the growth area. The dangling bond coverage then drops off rapidly near the edge of the growth area. A saturation of the dangling bond coverage over the middle of the Gaussian spatial profile of the electron beam is consistent with the saturation of the growth rate versus electron exposure time observed in Fig. 7.

GIXRD measurements of the Si EE-ALD films did not reveal any diffraction peaks. The GIXRD results are consistent with an amorphous structure for the Si EE-ALD films following atmospheric exposure. The extensive oxidation of the Si EE-ALD films revealed by the *ex situ* XPS depth profile measurements probably removed any crystallinity that may have been present prior to atmospheric exposure. In addition, the carbon impurities at ~10 at. % would also be expected to remove silicon crystallinity.

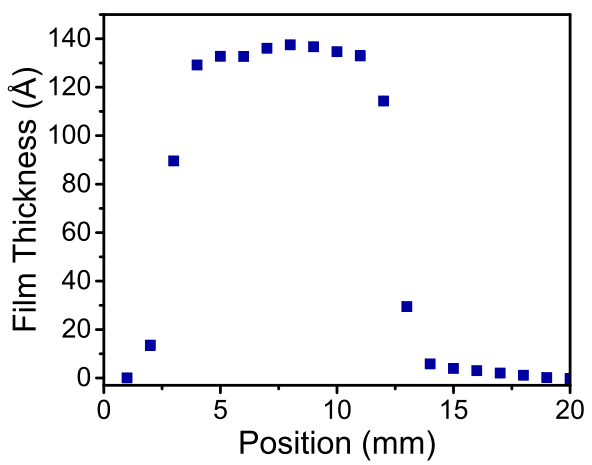

FIG. 11. (Color online) Film thickness vs spatial position for growth area observed in Fig. 10. Film thickness is uniform over most of the region exposed to the electron beam.

In situ capping of the silicon films may prevent oxidation and facilitate the observation of crystallinity. The crystallinity might also be observed by growing much thicker Si EE-ALD films that would prevent the diffusion of oxygen deep into the bulk of the silicon films. Improvements in film crystallinity should also be possible by producing higher purity silicon films through the reduction of residual hydrocarbon species in the vacuum chamber. The effect of residual hydrocarbon species is magnified by the delay between the production of dangling bonds by the electron flux and the subsequent Si_2H_6 exposure. The long wait times of 5 min required for the electron gun filament to cool probably contributed to higher carbon impurities in the Si EE-ALD films.

F. Comparison with earlier Si ALD and applications of Si EE-ALD

Si EE-ALD is able to deposit silicon at room temperature. In comparison, other reports of Si ALD have required much higher temperatures. These higher temperatures are needed for H_2 or HCl thermal desorption from the silicon surface. The initial report for Si ALD was performed at a high temperature of 825 °C using SiH_2Cl_2 and H_2 as the precursors.[57] Subsequent studies have questioned the mechanism for Si ALD suggested in this initial report.[58] The temperatures for Si ALD can be reduced to 540–610 °C using SiH_2Cl_2 together with H radicals.[58–60] In this Si ALD strategy, the chlorine coverage leads to self-limiting SiH_2Cl_2 adsorption and then H radicals allow the chlorine coverage to desorb as HCl.

Other Si ALD methods are also based on hydrogen desorption. Lower temperatures for Si ALD of 400 °C can be achieved using Si_2H_6 adsorption and He^+ ion bombardment to desorb hydrogen.[61] Si ALD has also been demonstrated using SiH_4 or Si_2H_6 adsorption and UV radiation to induce hydrogen desorption by a photothermal mechanism at 180–400 °C.[62–64] In addition, synchrotron radiation has been utilized to obtain Si ALD at 430–480 °C using Si_2H_6 adsorption followed by hydrogen desorption by photolytic and photothermal mechanisms.[65] Temperature modulation methods with low temperature SiH_4, Si_2H_6 or $SiH_2(CH_2CH_3)_2$ adsorption and H_2 desorption at ~550–700 °C have also been demonstrated for Si ALD.[66–68] None of these earlier Si ALD approaches can achieve Si ALD at room temperature.

Si EE-ALD should be useful to deposit ultrathin silicon films at room temperature. Low temperatures are required for silicon deposition on polymer and other thermally fragile substrates. Silicon deposited on polymer foils can be used to fabricate flexible silicon devices such as solar cells, displays, sensors and thin film transistors.[69–72] The silicon films could also be doped using hydrides, such as B_2H_6 and PH_3, that are good candidates for hydrogen ESD following their adsorption on silicon dangling bonds. The room temperature deposition of silicon will also allow the integration of silicon with other materials by eliminating thermal expansion mismatch problems that occur when cooling down from higher temperatures.

Low temperatures are also needed to deposit silicon on substrates that would react with silicon to form silicides at higher temperature. One key application is the fabrication of Mo/Si multilayers for extreme ultraviolet (EUV) mirrors.[73] The Mo/Si multilayer mirrors have high reflectivity at $\lambda = 13.5$ nm for EUV lithography for advanced semiconductor processing.[74] However, silicide formation at temperatures $>210\,^{\circ}$C causes interface roughness that degrades the reflectivity.[74,75] Silicon EE-ALD at low temperatures may provide extremely conformal silicon deposition and offer advantages to the sputter deposition techniques that are currently employed to fabricate the Mo/Si multilayer mirrors.[73]

In addition, there are other applications that may benefit from the directional properties of the electron flux during Si EE-ALD. If the electron flux is at normal incidence to the substrate, then surfaces that are parallel to the electron flux will receive very little flux compared with surfaces that are normal to the electron flux. For example, sidewalls of trenches may be parallel to the electron flux and receive very little flux. This geometry would favor "bottom-up" filling of the trench.[76] The Si EE-ALD would occur first at the bottom of the trench and proceed up the trench with negligible deposition on the sidewalls. This bottom-up filling could be useful for filling high aspect ratio structures.

IV. CONCLUSIONS

Silicon films were grown at room temperature using EE-ALD techniques with sequential exposures of disilane and low energy electrons in the range of 25–200 eV. The silicon film growth at low temperature results from hydrogen ESD on the silicon surface. The hydrogen removal forms dangling bonds that are able to adsorb Si_2H_6 during the subsequent Si_2H_6 exposure. The Si EE-ALD was self-limiting with respect to the Si_2H_6 exposure and the electron exposure time. The silicon films grew linearly with number of reaction cycles and growth rates of up to $\sim$0.3 Å/cycle were observed at electron energies of 100–150 eV. These growth rates are close to the expected growth rates assuming disilane adsorption on the dangling bonds on reconstructed single-crystal silicon surfaces.

The Si EE-ALD was dependent on the electron energy. Silicon growth had a threshold around 25 eV and showed a maximum growth rate between 100 and 150 eV. The silicon growth rate then decreased above 155 eV. There was a correlation between the silicon growth rates and the silicon core electron energies. This correlation argues that at least part of the silicon growth mechanism is related to electron removal from silicon core levels and the resulting Auger decay. Fitting the silicon growth rate versus electron exposure time yielded a hydrogen ESD cross section of $\sigma = 5.8 \times 10^{-17}$ cm^2.

The silicon films were grown using an electron flood gun that produced silicon film growth over areas of $\sim$1 cm^2. The silicon growth was very uniform over the area irradiated by the electron beam. The Si EE-ALD films contained carbon concentrations of $\sim$10 at. %. The carbon impurity is believed to result from residual hydrocarbons in the vacuum chamber that compete with disilane for the dangling bonds during silicon film growth. Si EE-ALD should find application for depositing ultrathin silicon films on thermally fragile substrates, preventing silicide formation, and for bottom up filling.

ACKNOWLEDGMENTS

This work was supported by Defense Advanced Research Projects Agency (DARPA) under Grant No. W911NF-13-1-0041. The authors thank Tyler McQuade and Anne Fischer from DARPA for their support and helpful comments. The authors also acknowledge Kenneth Smith and Donald David from the University of Colorado Integrated Instrument Development Facility for their help with system design, development, and computer interfacing. In addition, the authors thank Jonas Gertsch and Diane Lancaster for growing the ALD buffer layers.

[1]P. A. Coon, M. L. Wise, and S. M. George, J. Cryst. Growth **130**, 162 (1993).
[2]S. M. Gates and S. K. Kulkarni, Appl. Phys. Lett. **58**, 2963 (1991).
[3]J. M. Jasinski and S. M. Gates, Acc. Chem. Res. **24**, 9 (1991).
[4]J. L. Regolini, D. Bensahel, E. Scheid, and J. Mercier, Appl. Phys. Lett. **54**, 658 (1989).
[5]F. C. Eversteyn, Philips Res. Rep. **29**, 45 (1974).
[6]P. Gupta, V. L. Colvin, and S. M. George, Phys. Rev. B **37**, 8234 (1988).
[7]B. G. Koehler, C. H. Mak, D. A. Arthur, P. A. Coon, and S. M. George, J. Chem. Phys. **89**, 1709 (1988).
[8]R. Walsh, Acc. Chem. Res. **14**, 246 (1981).
[9]G. Schulze and M. Henzler, Surf. Sci. **124**, 336 (1983).
[10]M. L. Wise, B. G. Koehler, P. Gupta, P. A. Coon, and S. M. George, Surf. Sci. **258**, 166 (1991).
[11]K. Sinniah, M. G. Sherman, L. B. Lewis, W. H. Weinberg, J. T. Yates, and K. C. Janda, J. Chem. Phys. **92**, 5700 (1990).
[12]M. M. Albert and N. H. Tolk, Phys. Rev. B **63**, 035308 (2000).
[13]T. Fuse, T. Fujino, J.-T. Ryu, M. Katayama, and K. Oura, Surf. Sci. **420**, 81 (1999).
[14]N. Matsunami, Y. Hasebe, and N. Itoh, Surf. Sci. **192**, 27 (1987).
[15]P. R. Antoniewicz, Phys. Rev. B **21**, 3811 (1980).
[16]P. J. Feibelman and M. L. Knotek, Phys. Rev. B **18**, 6531 (1978).
[17]D. Menzel and R. Gomer, J. Chem. Phys. **41**, 3311 (1964).
[18]P. A. Redhead, Can. J. Phys. **42**, 886 (1964).
[19]T. E. Madey, Surf. Sci. **299**, 824 (1994).
[20]J. T. Yates, J. Chem. Phys. **137**, 091701 (2012).
[21]R. D. Ramsier and J. T. Yates, Surf. Sci. Rep. **12**, 246 (1991).
[22]J. J. Czyzewski, T. E. Madey, and J. T. Yates, Phys. Rev. Lett. **32**, 777 (1974).
[23]T. Yasue, A. Ichimiya, and S. Ohtani, Appl. Surf. Sci. **33/34**, 167 (1988).
[24]R. M. Wallace, P. A. Taylor, M. J. Dresser, W. J. Choyke, and J. T. Yates, Rev. Sci. Instrum. **62**, 720 (1991).
[25]A. L. Johnson, M. M. Walczak, and T. E. Madey, Langmuir **4**, 277 (1988).
[26]S. J. Randolph, J. D. Fowlkes, and P. D. Rack, Crit. Rev. Solid State Mater. Sci. **31**, 55 (2006).
[27]J. W. Lyding, T. C. Shen, J. S. Hubacek, J. R. Tucker, and G. C. Abeln, Appl. Phys. Lett. **64**, 2010 (1994).
[28]D. P. Adams, T. M. Mayer, and B. S. Swartzentruber, J. Vac. Sci. Technol., B **14**, 1642 (1996).
[29]P. Avouris, R. E. Walkup, A. R. Rossi, H. C. Akpati, P. Nordlander, T. C. Shen, G. C. Abeln, and J. W. Lyding, Surf. Sci. **363**, 368 (1996).
[30]T. Hitosugi, T. Hashizume, S. Heike, S. Watanabe, Y. Wada, T. Hasegawa, and K. Kitazawa, Jpn. J. Appl. Phys., Part 2 **36**, L361 (1997).
[31]T. C. Shen, C. Wang, G. C. Abeln, J. R. Tucker, J. W. Lyding, P. Avouris, and R. E. Walkup, Science **268**, 1590 (1995).
[32]J. N. Randall, J. W. Lyding, S. Schmucker, J. R. Von Ehr, J. Ballard, R. Saini, H. Xu, and Y. Ding, J. Vac. Sci. Technol., B **27**, 2764 (2009).
[33]T. C. Shen, C. Wang, J. W. Lyding, and J. R. Tucker, Appl. Phys. Lett. **66**, 976 (1995).
[34]J. B. Ballard *et al.*, J. Vac. Sci. Technol., B **32**, 041804 (2014).

[35]K. E. J. Goh, S. Chen, H. Xu, J. Ballard, J. N. Randall, and J. R. Von Ehr, Appl. Phys. Lett. **98**, 163102 (2011).
[36]J. H. G. Owen, J. Ballard, J. N. Randall, J. Alexander, and J. R. Von Ehr, J. Vac. Sci. Technol., B **29**, 06f201 (2011).
[37]J. K. Sprenger, A. S. Cavanagh, H. Sun, K. J. Wahl, A. Roshko, and S. M. George, Chem. Mater. **28**, 5282 (2016).
[38]M. Asif Khan, J. N. Kuznia, J. M. Van Hove, D. T. Olson, S. Krishnankutty, and R. M. Kolbas, Appl. Phys. Lett. **58**, 526 (1991).
[39]P. Gibart, Rep. Prog. Phys. **67**, 667 (2004).
[40]D. A. Neumayer and J. G. Ekerdt, Chem. Mater. **8**, 9 (1996).
[41]B.-C. Ahn, K. Shimizu, T. Satoh, H. Kanoh, O. Sugiura, and M. Matsumara, Jpn. J. Appl. Phys., Part 1 **30**, 3695 (1991).
[42]E. M. Oks and P. M. Schanin, Phys. Plasmas **6**, 1649 (1999).
[43]P. Poodt, D. C. Cameron, E. Dickey, S. M. George, V. Kuznetsov, G. N. Parsons, F. Roozeboom, G. Sundaram, and A. Vermeer, J. Vacuum Sci. Technol., A **30**, 010802 (2012).
[44]J. W. Klaus, S. J. Ferro, and S. M. George, Thin Solid Films **360**, 145 (2000).
[45]H. H. Madden, D. R. Jennison, M. M. Traum, G. Margaritondo, and N. G. Stoffel, Phys. Rev. B **26**, 896 (1982).
[46]K. R. Shepperd, C. D. Lane, and T. M. Orlando, J. Chem. Phys. **132**, 214704 (2010).
[47]K. Ueda, S. Kodama, and A. Takano, Surf. Sci. **283**, 195 (1993).
[48]A. C. Dillon, M. B. Robinson, and S. M. George, Surf. Sci. **295**, L998 (1993).
[49]K. J. Uram and U. Jansson, Surf. Sci. **249**, 105 (1991).
[50]S. M. Gates, Surf. Sci. **195**, 307 (1988).
[51]Y. M. Wu and R. M. Nix, Surf. Sci. **306**, 59 (1994).
[52]S. W. Ong, E. S. Tok, and H. C. Kang, J. Chem. Phys. **133**, 074708 (2010).
[53]M. Shinohara, M. Niwano, Y. Neo, and K. Yokoo, Thin Solid Films **369**, 16 (2000).
[54]C. Goeden and G. Dollinger, Appl. Surf. Sci. **147**, 107 (1999).
[55]T. E. Madey and J. T. Yates, J. Vac. Sci. Technol. **8**, 525 (1971).
[56]D. E. Aspnes and A. A. Studna, Phys. Rev. B **27**, 985 (1983).
[57]J. Nishizawa, K. Aoki, S. Suzuki, and K. Kikuchi, J. Electrochem. Soc. **137**, 1898 (1990).
[58]J. A. Yarmoff, D. K. Shuh, T. D. Durbin, C. W. Lo, D. A. Lapianosmith, F. R. McFeely, and F. J. Himpsel, J. Vac. Sci. Technol., A **10**, 2303 (1992).
[59]E. Hasunuma, S. Sugahara, S. Hoshino, S. Imai, K. Ikeda, and M. Matsumura, J. Vac. Sci. Technol., A **16**, 679 (1998).
[60]S. Imai, T. Iizuka, O. Sugiura, and M. Matsumura, Thin Solid Films **225**, 168 (1993).
[61]A. Mahajan, J. Irby, D. Kinosky, R. Qian, S. Thomas, S. Banerjee, A. Tasch, and T. Picraux, Thin Solid Films **225**, 177 (1993).
[62]D. Lubben, R. Tsu, T. R. Bramblett, and J. E. Greene, J. Vac. Sci. Technol., A **9**, 3003 (1991).
[63]J. Murota, M. Sakuraba, and S. Ono, Appl. Phys. Lett. **62**, 2353 (1993).
[64]Y. Suda, D. Lubben, T. Motooka, and J. E. Greene, J. Vac. Sci. Technol., B **7**, 1171 (1989).
[65]H. Akazawa and Y. Utsumi, J. Appl. Phys. **78**, 2725 (1995).
[66]P. A. Coon, M. L. Wise, A. C. Dillon, M. B. Robinson, and S. M. George, J. Vac. Sci. Technol., B **10**, 221 (1992).
[67]F. Hirose, M. Suemitsu, and N. Miyamoto, Appl. Surf. Sci. **60–61**, 592 (1992).
[68]J. Nishizawa, A. Murai, T. Ohizumi, T. Kurabayashi, K. Ohtsuka, and T. Yoshida, J. Cryst. Growth **209**, 327 (2000).
[69]Y. B. Chung, H. K. Park, D. K. Lee, W. Jo, J. H. Song, S. H. Lee, and N. M. Hwang, J. Cryst. Growth **327**, 57 (2011).
[70]C. Koch, M. Ito, and M. Schubert, Sol. Energy Mater. Sol. Cells **68**, 227 (2001).
[71]S. H. Lee, J. S. Jung, S. S. Lee, S. B. Lee, and N. M. Hwang, J. Cryst. Growth **453**, 151 (2016).
[72]M. B. Schubert, Thin Solid Films **337**, 240 (1999).
[73]T. W. Barbee, S. Mrowka, and M. C. Hettrick, Appl. Opt. **24**, 883 (1985).
[74]S. Yulin, N. Benoit, T. Feigl, and N. Kaiser, Microelectron. Eng. **83**, 692 (2006).
[75]H.-J. Voorma, E. Louis, N. B. Koster, and F. Bijkerk, J. Appl. Phys. **83**, 4700 (1998).
[76]T. P. Moffat and D. Josell, J. Electrochem. Soc. **159**, D208 (2012).